Available online at www.sciencedirect.com
SCIENCE DIRECT®
Composite Structures 72 (2006) 321–329
COMPOSITE STRUCTURES
www.elsevier.com/locate/compstruct

Comparison of some improved solutions for mixed-mode composite delamination coupons

András Szekrényes *, József Uj

Department of Applied Mechanics, Budapest University of Technology and Economics, H-1521 Budapest, POB 11, Hungary

Available online 22 February 2005

Abstract

Four different solutions for the energy release rate of orthotropic, beam-like fracture specimens were compared in the present work. Two beam theory-based approaches were utilized. The current authors developed one of them, the other one was previously published in the literature. A model based on refined plate theory was also considered. Finally equations based on a numerical calibration technique were utilized as a fourth solution. These solutions were extended for the case of composite double-cantilever beam, end-loaded split, single-leg bending and mixed-mode bending fracture specimens. Comparison between the different solutions shows somewhat distinct results, especially for the mode ratio. There are some explanations for the experienced discrepancies between the mentioned solutions.

Keywords: Beam theory; Strain energy release rate; Mode ratio; Delamination

1. Introduction

The interlaminar fracture is primary failure mode in laminated composite structures. The interlaminar fracture toughness (known as the resistance to delamination) is determined through specimens, which behave as slender beams. The double-cantilever beam (DCB) is a standard specimen for measuring the mode-I delamination toughness. Numerous beam theory-based solutions were developed in the literature, which incorporates the Winkler foundation, Timoshenko beam theory and Saint Venant effect [1–3]. For mode-II specimens beam theory [4,5] and the finite element method [6] was applied to obtain improved solutions for the strain energy release rate. The solution by Wang and Qiao [7] for the end-notched flexure (ENF) specimen should be mentioned due to its elegance and simplicity. For mode-II testing the four-point bend end notched flexure (4ENF) [8], the mode-II end-loaded split (ELS) [9] and the over-notched flexure (ONF) [10] coupons are available. Also, for mixed-mode I/II testing many configurations were developed by the researchers. See for instance the cracked-lap shear (CLS) [11], the mixed-mode end-loaded split (ELS) [12,13], the single-leg bending (SLB) [14–16] and its twin brother, the mixed-mode flexure (MMF) [17,18] specimens. Some other configurations were reviewed by Reeder and Crews [19], Suo [20] and Tracy et al. [21]. None of them is able to vary the mode ratio within a wide range. The standard mixed-mode bending (MMB) was originally developed by Reeder and Crews [19]. Since this configuration enables the variation of the mode ratio and to obtain a complete fracture envelope it is intensively applied in nowadays [22,23]. The MMB specimen has several disadvantages, especially that it requires a complex fixture. On the other hand only complex beam theory-based reduction technique can be applied. In some cases, for example in multidirectional laminates due to the discrepancies between manufactured and predicted bending and torsional stiffnesses

* Corresponding author. Tel.: +36 1 463 1170; fax: +36 1 463 3471.
E-mail addresses: szeki@mm.bme.hu (A. Szekrényes), uj@mm.bme.hu (J. Uj).

0263-8223/$ - see front matter © 2005 Elsevier Ltd. All rights reserved.
doi:10.1016/j.compstruct.2005.01.002

the analytical equations may give misleading results. Hence the MMB is accepted mainly for the testing of unidirectional laminates. Also, other-type of mixed-mode configurations are applied in nowadays. Davidson et al. [15] applied the SLB specimen to investigate the interlaminar fracture in multidirectional laminates. The great advantage of this test is that the SLB may be performed in a simple three-point fixture and the compliance calibration (CC) method applies. The ELS specimen is suitable to investigate crack propagation and fiber-bridging under mixed-mode condition [24]. Improved beam theory-based solutions were obtained in our last work for the SLB and ELS coupons [25]. The role of material orthotropy on the fracture toughness of certain composite specimens was investigated by Bao et al. [26]. In their work closed-form equations were derived based on numerical calculations for the DCB, the mode-II ELS and the mixed-mode ELS specimens.

Under mixed-mode I/II condition the mode decomposition is an important issue. Different methods were developed by the researchers to solve this problem. The beam theory-based global method was developed by Williams [27], while the local method was composed by Suo and Hutchinson [28]. The crack tip element analysis is a third analytical method [29,30], which is equivalent to the local approach. In the work of Bruno and Greco a refined plate model including shear effect was applied, the individual mode components were evaluated by using the interlaminar stresses and displacements [31,32]. This method was found to give the same result as Williams' global approach. The global method was improved with the effect of Winkler foundation and transverse shear in [25]. The local method was completed with shear effect by Wang and Qiao [33] and notable contribution from shear-bending coupling was found. Finally the virtual crack-closure technique (VCCT) should be mentioned, which is widely applied for mode decomposition and energy release rate calculation [34,35].

In the current work the DCB, SLB, ELS and MMB specimens are examined. Four different solutions are extended for these fracture specimens including mode-mixity analysis: beam theory-based solution I [25,36] and II [2,5,19], solution based on refined plate theory [31,32] and a numerical solution by Bao et al. [26]. Furthermore mode decomposition based on the VCCT [34] was achieved in all the three mixed-mode specimens. The delamination coupons are illustrated in Fig. 1.

2. Beam theory-based solution I

Based on previous works [2,25,36], the following equations may be derived based on Williams' global method [27] for the individual energy release rate components of composite specimens under general mixed-mode I/II loading condition:

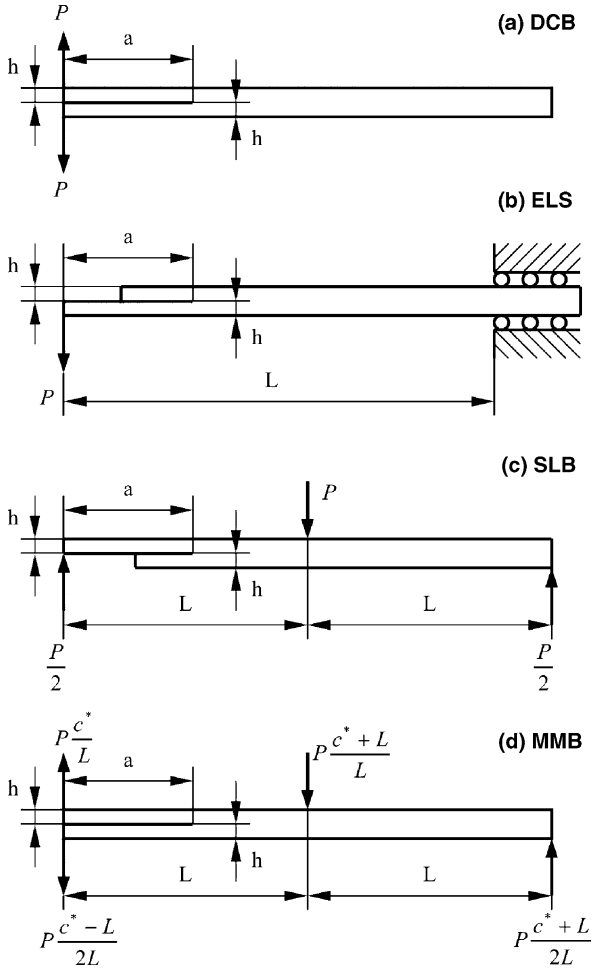

Fig. 1. Delamination specimens.

$$G_{\mathrm{I}} = \frac{M_{\mathrm{I}}^2(12 + f_{\mathrm{WP2}} + f_{\mathrm{SV2}} + f_{\mathrm{T2}})}{b^2 h^3 E_{11}}, \tag{1}$$

$$G_{\mathrm{II}} = \frac{M_{\mathrm{II}}^2(9 + f_{\mathrm{SH2}})}{b^2 h^3 E_{11}}, \tag{2}$$

where the functions in Eqs. (1) and (2) are:

$$f_{\mathrm{WP2}} = 6.64\left(\frac{h}{a}\right)\left(\frac{E_{11}}{E_{33}}\right)^{\frac{1}{4}} + 3.68\left(\frac{h}{a}\right)^2\left(\frac{E_{11}}{E_{33}}\right)^{\frac{1}{2}}, \tag{3}$$

$$f_{\mathrm{SV2}} = \frac{12}{\pi}\left(\frac{h}{a}\right)\left(\frac{E_{11}}{G_{13}}\right)^{\frac{1}{2}}, \tag{4}$$

$$f_{\mathrm{T2}} = \frac{1}{k}\left(\frac{h}{a}\right)^2\left(\frac{E_{11}}{G_{13}}\right), \tag{5}$$

$$f_{\mathrm{SH2}} = 1.96\left(\frac{h}{a}\right)\left(\frac{E_{11}}{G_{13}}\right)^{\frac{1}{2}} + 0.43\left(\frac{h}{a}\right)^2\left(\frac{E_{11}}{G_{13}}\right), \tag{6}$$

where Eq. (3) incorporates the effect of Winkler–Pasternak foundation, Eq. (4) takes the Saint Venant effect into account, while Eq. (5) accounts for transverse shear effect and Eq. (6) considers shear deformation of the crack tip. Furthermore in Eq. (5) $k = 5/6$ is the shear correction factor. The mode-I and mode-II bending moments may be obtained as follows [27]:

$$M_{\mathrm{I}} = (M_1 - M_2)/2, \quad M_{\mathrm{II}} = (M_1 + M_2)/2, \tag{7}$$

where M_1 and M_2 are reduced bending moments at the crack tip. The subscript refers to the upper (1) and lower (2) specimen arm.

In the case of the DCB specimen (see Fig. 1a) the bending moments at the crack tip are $M_1 = -Pa$, $M_2 = Pa$. Thus the energy release rate from Eq. (1) becomes:

$$G_{\mathrm{I}}^{\mathrm{DCB}} = \frac{12P^2a^2}{b^2h^3E_{11}}\left[1+0.55\left(\frac{h}{a}\right)\left(\frac{E_{11}}{E_{33}}\right)^{\frac{1}{4}}+0.31\left(\frac{h}{a}\right)^2\left(\frac{E_{11}}{E_{33}}\right)^{\frac{1}{2}} + 0.32\left(\frac{h}{a}\right)\left(\frac{E_{11}}{G_{13}}\right)^{\frac{1}{2}}+0.1\left(\frac{h}{a}\right)^2\left(\frac{E_{11}}{G_{13}}\right)\right]. \tag{8}$$

Let us consider the case of the mixed-mode ELS coupon in Fig. 1b, whereas: $M_1 = 0$, $M_2 = Pa$, from Eqs. (1) and (2) we obtain:

$$G_{\mathrm{I}}^{\mathrm{ELS}} = \frac{12P^2a^2}{4b^2h^3E_{11}}\left[1+0.55\left(\frac{h}{a}\right)\left(\frac{E_{11}}{E_{33}}\right)^{\frac{1}{4}}+0.31\left(\frac{h}{a}\right)^2 \times\left(\frac{E_{11}}{E_{33}}\right)^{\frac{1}{2}}+0.32\left(\frac{h}{a}\right)\left(\frac{E_{11}}{G_{13}}\right)^{\frac{1}{2}}+0.1\left(\frac{h}{a}\right)^2\left(\frac{E_{11}}{G_{13}}\right)\right], \tag{9}$$

$$G_{\mathrm{II}}^{\mathrm{ELS}} = \frac{9P^2a^2}{4b^2h^3E_{11}}\left[1+0.22\left(\frac{h}{a}\right)\left(\frac{E_{11}}{G_{13}}\right)^{\frac{1}{2}}+0.048\left(\frac{h}{a}\right)^2\left(\frac{E_{11}}{G_{13}}\right)\right]. \tag{10}$$

In the case of the SLB specimen (Fig. 1c) $M_1 = -Pa/2$, $M_2 = 0$, from Eqs. (1) and (2) we obtain:

$$G_{\mathrm{I}}^{\mathrm{SLB}} = \frac{12P^2a^2}{16b^2h^3E_{11}}\left[1+0.55\left(\frac{h}{a}\right)\left(\frac{E_{11}}{E_{33}}\right)^{\frac{1}{4}} +0.31\left(\frac{h}{a}\right)^2\left(\frac{E_{11}}{E_{33}}\right)^{\frac{1}{2}}+0.32\left(\frac{h}{a}\right)\left(\frac{E_{11}}{G_{13}}\right)^{\frac{1}{2}}+0.1\left(\frac{h}{a}\right)^2\left(\frac{E_{11}}{G_{13}}\right)\right], \tag{11}$$

$$G_{\mathrm{II}}^{\mathrm{SLB}} = \frac{9P^2a^2}{16b^2h^3E_{11}}\left[1+0.22\left(\frac{h}{a}\right)\left(\frac{E_{11}}{G_{13}}\right)^{\frac{1}{2}}+0.048\left(\frac{h}{a}\right)^2\left(\frac{E_{11}}{G_{13}}\right)\right]. \tag{12}$$

For the MMB (Fig. 1d) specimen $M_1 = Pc^*a/L$, $M_2 = P(c^* - L)a/2L$, thus we have:

$$G_{\mathrm{I}}^{\mathrm{MMB}} = \frac{12P^2a^2(3c^*-L)^2}{16b^2h^3E_{11}L^2}\left[1+0.55\left(\frac{h}{a}\right)\left(\frac{E_{11}}{E_{33}}\right)^{\frac{1}{4}}+0.31\left(\frac{h}{a}\right)^2 \times\left(\frac{E_{11}}{E_{33}}\right)^{\frac{1}{2}}+0.32\left(\frac{h}{a}\right)\left(\frac{E_{11}}{G_{13}}\right)^{\frac{1}{2}}+0.1\left(\frac{h}{a}\right)^2\left(\frac{E_{11}}{G_{13}}\right)\right], \tag{13}$$

$$G_{\mathrm{II}}^{\mathrm{MMB}} = \frac{9P^2a^2(c^*+L)^2}{16b^2h^3E_{11}L^2}\left[1+0.22\left(\frac{h}{a}\right)\left(\frac{E_{11}}{G_{13}}\right)^{\frac{1}{2}} + 0.048\left(\frac{h}{a}\right)^2\left(\frac{E_{11}}{G_{13}}\right)\right]. \tag{14}$$

The mode ratio ($G_{\mathrm{I}}/G_{\mathrm{II}}$) in each case may be obtained by combining the equations above.

3. Beam theory-based solution II

The classical solution of Williams [1] for the mode-I DCB specimen was improved with transverse shear and Saint Venant effect by Olsson [3]. On the other hand Carlsson et al. [5] performed an improved analysis for the mode-II ENF specimen using Timoshenko beam theory. Later Reeder and Crews [19] obtained a solution for the MMB specimen combining the solutions by Williams and Carlsson et al. The MMB specimen was treated as the superposition of the DCB and ENF specimens. Combining the results of these works the following expressions may be derived for the energy release rate components:

$$G_{\mathrm{I}} = \frac{M_{\mathrm{I}}^2(12 + f_{\mathrm{W}} + f_{\mathrm{SV2}} + f_{\mathrm{T2}})}{b^2h^3E_{11}}, \tag{15}$$

$$G_{\mathrm{II}} = \frac{M_{\mathrm{II}}^2(9 + f_{\mathrm{SH}})}{b^2h^3E_{11}}, \tag{16}$$

where

$$f_{\mathrm{W}} = 15.36\left(\frac{h}{a}\right)\left(\frac{E_{11}}{E_{33}}\right)^{\frac{1}{4}} + 4.92\left(\frac{h}{a}\right)^2\left(\frac{E_{11}}{E_{33}}\right)^{\frac{1}{2}}, \tag{17}$$

$$f_{\mathrm{SH}} = 1.8\left(\frac{h}{a}\right)^2\left(\frac{E_{11}}{G_{13}}\right). \tag{18}$$

The equations above will be referred to as the solutions by Carlsson and Olsson. The mode-I and mode-II bending moments are the same as those mentioned in Section 2.

4. Solution based on numerical calibration

Bao et al. [26] derived the energy release rate components based on finite element calculations for certain

composite specimens. The following generalized expressions can be obtained using their equations:

$$G_{\mathrm{I}} = \frac{12M_{\mathrm{I}}^2 Y_{\mathrm{I}}^2}{b^2 h^3 E_{11}}, \tag{19}$$

$$G_{\mathrm{II}} = \frac{9M_{\mathrm{II}}^2 Y_{\mathrm{II}}^2}{b^2 h^3 E_{11}}, \tag{20}$$

where

$$Y_{\mathrm{I}} = 1 + (0.677 + 0.146\beta - 0.0178\beta^2 + 0.00242\beta^3)\lambda^{-\frac{1}{4}}\left(\frac{h}{a}\right), \tag{21}$$

$$Y_{\mathrm{II}} = 1 + (0.206 + 0.0761\beta - 0.00978\beta^2 + 0.00112\beta^3)\lambda^{-\frac{1}{4}}\left(\frac{h}{a}\right), \tag{22}$$

$$\lambda = \frac{E_{33}}{E_{11}}, \quad \beta = \frac{(E_{11}E_{33})^{\frac{1}{2}}}{2G_{13}} - (v_{13}v_{31})^{\frac{1}{2}} - 1. \tag{23}$$

The above solution is based on the principle of superposition, for instance the solution for the mixed-mode ELS specimen was obtained as the sum of the mode-I DCB and the mode-II ELS specimens.

5. Solution based on a refined plate model

Bruno and Greco [31,32] utilized a linear elastic interface model between two Reissner–Mindlin plates. Their solution can be simply extended for any mixed-mode coupons. The solution after some transformations can be written as:

$$G_{\mathrm{I}} = \frac{M_{\mathrm{I}}^2(12 + f_{\mathrm{BS}} + f_{\mathrm{T2}})}{b^2 h^3 E_{11}}, \tag{24}$$

$$G_{\mathrm{II}} = \frac{9M_{\mathrm{II}}^2}{b^2 h^3 E_{11}}, \tag{25}$$

$$f_{\mathrm{BS}} = 7.59\left(\frac{h}{a}\right)\left(\frac{E_{11}}{G_{13}}\right)^{\frac{1}{4}}. \tag{26}$$

It should be noted that this formulation gives equivalent result to the simple beam theory with respect to the mode-II component, as it can be seen from Eq. (25).

6. Mode decomposition using the VCCT method

For the mixed-mode specimens a series of FE models were constructed to obtain mode ratios within reasonable crack length ranges. The models were developed in the commercial code COSMOS/M 2.0 using PLANE2D elements under plane stress state, which is consistent with beam formulation of the problems. The specimens were 150 mm long, $b = 20$ mm wide and $2h = 6.1$ mm thick. The material properties are given for glass/polyester composite specimens, which were manufactured in our laboratory. The flexural modulus of the specimens were determined through a non-standard three-point bending test, which resulted in $E_{11} = 33$ GPa. Additional material properties were predicted by means of Niederstadt's [37] approximate rule of mixture: $E_{33} = 7.2$ GPa, $G_{13} = 3$ GPa and $v_{13} = v_{31} = 0.27$. According to the VCCT method the energy release rate components are [34]:

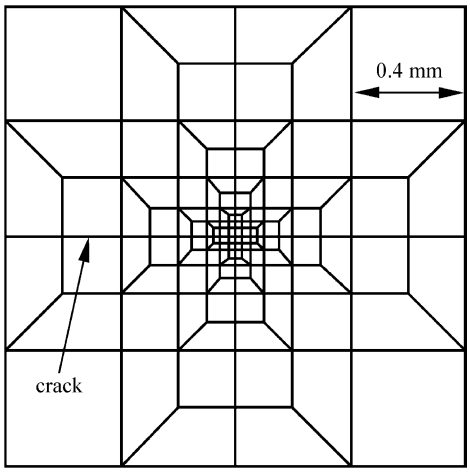

Fig. 2. FE mesh around the crack tip.

$$G_{\mathrm{I}} = \frac{1}{2b\Delta a}F_y(v_1 - v_2), \tag{27}$$

$$G_{\mathrm{II}} = \frac{1}{2b\Delta a}F_x(u_1 - u_2), \tag{28}$$

where F_x, F_y are nodal forces at the crack tip, v_1, v_2, u_1, u_2 are nodal displacements from Δa distance to the crack tip and b is the specimen width. A finite element mesh around the crack tip, suggested by Davidson and Sundararaman [16] was constructed, as it is shown in Fig. 2. Crack tip elements with finite crack extension of $\Delta a = 0.025$ mm were used (Fig. 2).

7. Results

All the equations were normalized with the results of Euler–Bernoulli beam theory. These are the first terms in Eqs. (8)–(14). The normalized strain energy release rates are plotted against the normalized crack length.

The results for the DCB and ELS specimens are illustrated in Fig. 3a and b, respectively. Fig. 4a and b present the same results for the SLB and MMB coupons. For all the four specimens essentially the same trends were obtained. An immediate observation is that the model by Carlsson–Olsson proves the largest improve-

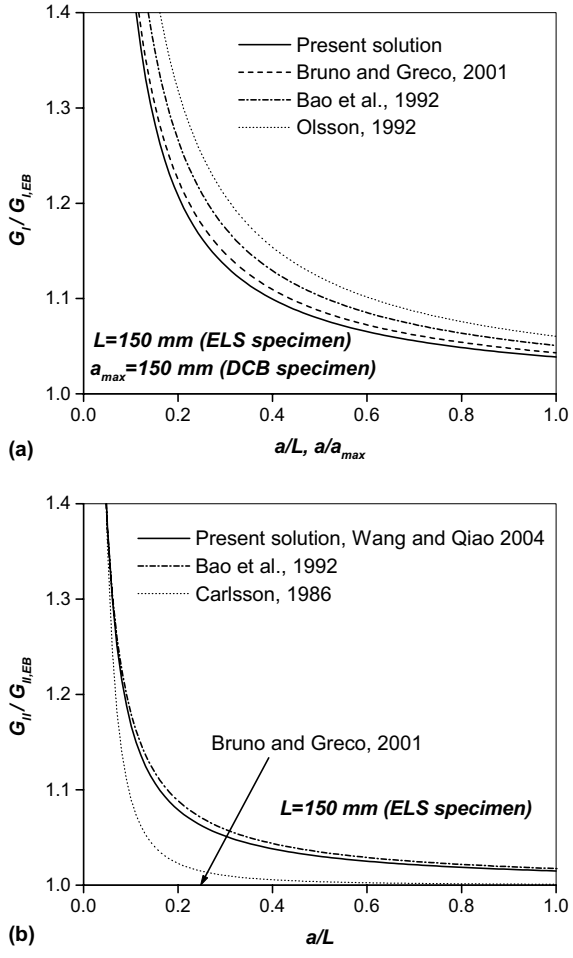

Fig. 3. Comparison of the mode-I (a) and mode-II (b) energy release rates for the DCB and ELS specimens.

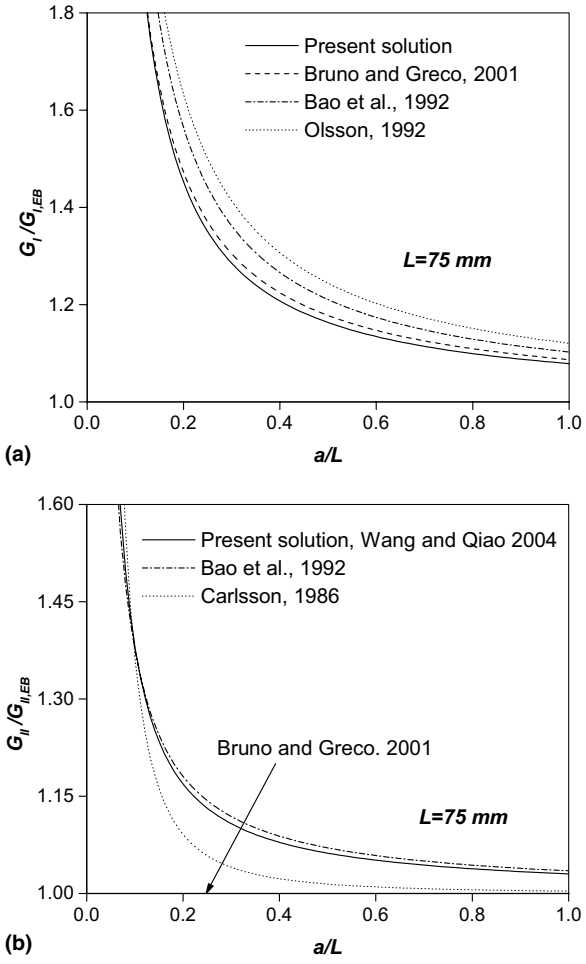

Fig. 4. Comparison of the mode-I (a) and mode-II (b) energy release rates for the SLB and MMB specimens.

ment for the mode-I component, which is somewhat surprising. The plate model by Bruno and Greco gives a curve, which is quite close to our solution. The normalized mode-II component is presented in Figs. 3b and 4b. The agreement was excellent between our model and the one by Bao et al. In contrast, the mode-II component is equivalent to the formula of Euler–Bernoulli beam model in accordance with the formulation of Bruno and Greco. Although the model by Carlsson provides some correction for the mode-II component, it is clear, that our solution seems to be more reasonable.

The mode ratios for the ELS specimen by five different approximations are compiled in Table 1. Slightly distinct results were obtained even in this case. The models by Bruno and Greco and Carlsson and Olsson show large mode-I dominance. Bao's numerical formulation shows

Table 1
Mode ratios (G_I/G_{II}) by different methods, ELS specimen

a [mm]	20	30	40	50	60	70	80	90	100
	1.574	1.493	1.452	1.428	1.412	1.401	1.392	1.386	1.380[a]
	1.846	1.654	1.559	1.516	1.483	1.461	1.445	1.432	1.421[b]
	1.693	1.566	1.500	1.469	1.445	1.429	1.417	1.408	1.400[c]
	1.893	1.719	1.626	1.569	1.530	1.502	1.481	1.465	1.452[d]
	1.250	1.176	1.144	1.120	1.105	1.093	1.085	1.078	1.073[e]

[a] Present.
[b] Ref. [31].
[c] Ref. [26].
[d] Ref. [5,2].
[e] VCCT.

Table 2
Mode ratios (G_I/G_{II}) by different methods, SLB specimen

a [mm]	20	30	40	50	60	70
	1.574	1.493	1.452	1.428	1.412	1.401[a]
	1.846	1.654	1.559	1.516	1.483	1.461[b]
	1.693	1.566	1.500	1.469	1.445	1.429[c]
	1.893	1.719	1.626	1.569	1.530	1.502[d]
	1.658	1.572	1.529	1.502	1.493	1.483[e]

[a] Present.
[b] Ref. [31].
[c] Ref. [26].
[d] Ref. [5,2].
[e] VCCT.

Table 3
Mode ratios (G_I/G_{II}) by different methods, MMB specimen

a [mm]	25	30	40	50	60	70
$c^* = 30$	0.031	0.030	0.030	0.029	0.029	0.029[a]
	0.035	0.033	0.032	0.031	0.030	0.030[b]
	0.033	0.032	0.031	0.030	0.029	0.030[c]
	0.037	0.035	0.033	0.032	0.031	0.031[d]
	0.179	0.175	0.173	0.175	0.175	0.177[e]
$c^* = 60$	0.922	0.903	0.878	0.864	0.854	0.847[a]
	1.025	0.987	0.940	0.913	0.895	0.882[b]
	0.965	0.938	0.906	0.886	0.873	0.863[c]
	1.083	1.040	0.983	0.949	0.925	0.909[d]
	1.102	1.066	1.038	1.025	1.015	1.018[e]
$c^* = 90$	2.130	2.084	2.028	1.994	1.972	1.956[a]
	2.367	2.279	2.171	2.107	2.065	2.036[b]
	2.227	2.166	2.091	2.045	2.015	1.993[c]
	2.500	2.400	2.270	2.191	2.137	2.098[d]
	2.078	2.015	1.962	1.929	1.914	1.914[e]
$c^* = 120$	3.257	3.188	3.101	3.050	3.016	2.992[a]
	3.621	3.486	3.320	3.223	3.159	3.113[b]
	3.406	3.313	3.197	3.128	3.081	3.048[c]
	3.469	3.372	3.246	3.169	3.116	3.078[d]
	2.843	2.759	2.686	2.637	2.620	2.616[e]

[a] Present.
[b] Ref. [31].
[c] Ref. [26].
[d] Ref. [5,2].
[e] VCCT.

good agreement with our results. Finally the plane stress FE model also shows some crack length dependence of the mode ratio but the mode-I dominance is not as significant here as in any of the former cases.

Table 2 presents the results for the SLB specimen. In this respect our solution matches well with Bao's solution and the result of the VCCT. Notice that the mode ratios by the closed-form solutions are the same as they are in the case of the ELS specimen.

In Table 3 the mode ratios are collected at four different lever length (c^*) values for the MMB specimen. At $c^* = 30$ mm some discrepancies were recognized between the closed-form solutions and the results of the VCCT method, maybe the lever length is not long enough in this case to open the crack in a sufficient degree. Our solution and the VCCT closely agree at the other lever lengths, not only in the case of the numerical values, but also in the case of the dependence of the mode ratio. All the other solutions show significant crack length dependence.

Summary of the results indicates the mode ratio depends on the method applied for calculation. Moreover the VCCT method shows the best correlation with our solution in case of the MMB specimen.

8. Discussion

As a consequence, the different solutions give distinct results, which should be clarified.

Table 4
Corrections for the DCB specimen from elastic foundation ($G_I/G_{I,EB}$)

a [mm]	20	30	40	50	60	70	80	90	100
	1.223	1.144	1.114	1.086	1.071	1.061	1.053	1.047	1.042[a]
	1.139	1.089	1.066	1.052	1.043	1.037	1.032	1.028	1.025[b]
	1.306	1.199	1.148	1.118	1.097	1.083	1.073	1.064	1.058[c]

[a] Present FE.
[b] Present analytical.
[c] Ref. [2].

According to the present formulation the total strain energy release rate was obtained by a superposition scheme, which incorporates the effect of Winkler–Pasternak-foundation, Saint Venant effect, transverse shear and crack tip deformation. Interaction between them was neglected, but the mode-I and mode-II components are equally supported by reasonable values.

We may assume that Bao's numerical model provides the more accurate result. Their model incorporates all the former effects and the possible interaction between them.

The refined plate model by Bruno and Greco affirms the significance of bending–shear interaction. Their model does not provide improved solution for the mode-II component, whereas our and Bao's solution show that the mode-II component should be contributed apart from simple beam theory. Thus, the overestimated mode ratios may be explained by the lack of correction for the mode-II component.

The combined solution by Carlsson and Olsson is based on similar considerations as our beam model. In our previous work [25] the elastic foundation was derived based on a general loading scheme for mixed-mode condition, where Steiner's theorem was considered. Consequently, this effect was ignored in Olsson's equations, the model does not account for Steiner's theorem in the case of the elastic foundation and so, it causes the discrepancy between Eqs. (3) and (17). Apart from that the mode-II component by Carlsson is only slightly contributed in comparison with our and Bao's solution. This may cause again overprediction in the mode ratio.

It should be kept in mind that in the case of the VCCT method the convergence and accuracy of the solution is not guaranteed due to the singularity nature of the problem. The results are sensitive to the size and number of finite elements around the crack tip. Furthermore the mesh refinement around the crack tip involves increase in the mode-II component.

9. Some explanations

In order to clarify the above discrepancies the finite element model of the DCB specimen may be utilized. The correction of the energy release rate is determined based on the work by Wang and Williams [6]. The model by Carlsson and Olsson indicates a very large improving effect from elastic foundation in the case of the mode-I component. Apart from that, the Saint Venant and transverse shear effects are also considered in this model. In our model the enhancing effect induced by the Winkler–Pasternak foundation is smaller in comparison with the model by and Olsson (refer to Figs. 3a and 4a). To find out which solution seems to be more reasonable a finite element analysis was carried out on DCB specimens where the shear moduli tended to infinity (G_{13} = 100,000 GPa). In this case the Saint Venant and transverse shear effect is eliminated, since according to Eqs. (4) and (5) the related correction functions become zero, and consequently the remained correction may be related to the elastic foundation. The results of this analysis are compiled in Table 4, indicating that the effect of elastic foundation is smaller than those provided by the classical elastic foundation model at each crack length. Our approach proves slightly smaller values from Winkler–Pasternak foundation analysis in comparison with the FE results, but it seems to be reasonable.

In the case of the mixed-mode specimens it is assumed that the solution may be obtained based on the principle of superposition. In the work by Bao et al. [26] an inverse superposition scheme was applied to the mixed-mode ELS specimen, i.e. the solution for the mixed-mode ELS and the mode-I DCB specimen was obtained, while the mode-II component was calculated by subtracting the latter from the former. This method yielded the same result as the traditionally applied principle, i.e. the combination of the mode-I DCB and mode-II ELS specimens. This may mean that the correction of the mode-I component should be the same in pure mode-I and in mixed-mode cases.

10. Conclusions

A comparative study was performed using four different solutions for the energy release rate of common delamination specimens, such as the mode-I DCB and the mixed-mode ELS, SLB and MMB specimens.

Furthermore the mode ratio was evaluated by the VCCT method in plane stress finite element models.

Comparison of the results shows somewhat different consequences. If only pure mode-I condition is investigated our and Bruno and Greco's solution (more or less) closely agree with that by Bao et al. On the contrary the previously developed solution by Olsson shows a little overprediction in comparison with Bao's numerical model. The mode-II component is only slightly contributed in accordance with Carlsson. In the model by Bruno and Greco the mode-II component suffers from any improvements apart from Euler–Bernoulli beam theory. Considering the mode ratios for the ELS specimen the present solution and the one by Bao et al. seems to be in good agreement. This is true also for the SLB specimen, and in this case also the VCCT method closely agrees with them. It should be mentioned that Steiner's theorem was ignored in the solution by Olsson with respect to the elastic foundation. Consequently, the mode ratio is overpredicted by this solution. In contrast for the MMB specimen the best agreement was found between the VCCT and our solution. As a consequence, the mode ratio depends on the technique applied for evaluation. Finally an approximate FE analysis was performed on the models of the DCB specimen and it was found that Steiner's theorem is necessary to be considered in order to obtain a reasonable correction.

Acknowledgments

This research work was supported by the fund OTKA T037324. The authors grateful to Tonny Nyman for providing the references by Yoon and Hong [14], Williams [27] and Raju et al. [34]. We wish to thank Barry D. Davidson for sending his work [16] to us.

References

[1] Williams JG. End corrections for orthotropic DCB specimens. Compos Sci Technol 1989;35:367–76.
[2] Olsson R. A simplified improved beam analysis of the DCB specimen. Compos Sci Technol 1992;43:329–38.
[3] Ozdil F, Carlsson LA, Davies P. Beam analysis of angle-ply laminate DCB specimens. Compos Sci Technol 1999;59:305–15.
[4] Ozdil F, Carlsson LA, Davies P. Beam analysis of angle-ply laminate end-notched flexure specimens. Compos Sci Technol 1998;58:1929–38.
[5] Carlsson LA, Gillespie JW, Pipes RB. On the analysis and design of the end notched flexure (ENF) specimen for mode II testing. J Compos Mater 1986;20:594–604.
[6] Wang Y, Williams JG. Corrections for mode II fracture toughness specimens of composite materials. Compos Sci Technol 1992;43:251–6.
[7] Wang J, Qiao P. Novel beam analysis of the end notched flexure specimen for mode-II fracture. Eng Fract Mech 2004;71:219–31.
[8] Schuecker C, Davidson BD. Evaluation of the accuracy of the four-point bend end-notched flexure test for mode II delamination toughness determination. Compos Sci Technol 2000;60:2137–46.
[9] Wang H, Vu-Khanh T. Use of end-loaded-split (ELS) test to study stable fracture behaviour of composites under mode-II loading. Compos Struct 1996;36:71–9.
[10] Wang W-X, Takao Y, Nakata M. Effects of friction on the measurement of the mode II interlaminar fracture toughness of composite laminates. In: Proceedings of the 14th International Conference on Composite Materials, San Diego, California, USA, 14–18 July, 2003.
[11] Lai Y-H, Rakestraw MD, Dillard DA. The cracked lap shear specimen revisited—a closed form solution. Int J Solids Struct 1996;33:1725–43.
[12] Hashemi S, Kinloch J, Williams JG. The effects of geometry, rate and temperature on mode I, mode II and mixed-mode I/II interlaminar fracture toughness of carbon-fibre/poly(ether–ether ketone) composites. J Compos Mater 1990;24:918–56.
[13] Hashemi S, Kinloch J, Williams JG. Mechanics and mechanisms of delamination in a poly(ether sulphone)-fibre composite. Compos Sci Technol 1990;37:429–62.
[14] Yoon SH, Hong CS. Modified end notched flexure specimen for mixed mode interlaminar fracture in laminated composites. Int J Fract 1990;43:R3–9.
[15] Davidson BD, Krüger R, König M. Three-dimensional analysis of center-delaminated unidirectional and multidirectional single-leg bending specimens. Compos Sci Technol 1995;54:385–94.
[16] Davidson BD, Sundararaman V. A single leg bending test for interfacial fracture toughness determination. Int J Fract 1996;78:193–210.
[17] Albertsen H, Ivens J, Peters P, Wevers M, Verpoest I. Interlaminar fracture toughness of CFRP influenced by fiber surface treatment: Part 1. Experimental results. Compos Sci Technol 1995;54:133–45.
[18] Korjakin A, Rikards R, Buchholz F-G, Wang H, Bledzki AK, Kessler A. Comparative study of interlaminar fracture toughness of GFRP with different fiber surface treatments. Polym Compos 1998;19:793–806.
[19] Reeder JR, Crews JR. Mixed-mode bending method for delamination testing. AIAA J 1990;28:1270–6.
[20] Suo Z. Delamination specimens for orthotropic materials. J Appl Mech 1990;57:627–34.
[21] Tracy GD, Feraboli P, Kedward KT. A new mixed mode test for carbon/epoxy composite systems. Compos Part A: Appl Sci Manufact 2003;34:1125–31.
[22] Kim BW, Mayer AH. Influence of fiber direction and mixed-mode ratio on delamination fracture toughness of carbon/epoxy laminates. Compos Sci Technol 2003;63:695–713.
[23] Chen JH, Sernow R, Schulz G, Hinrichsen G. A modification of the mixed-mode bending test apparatus. Compos Part A: Appl Sci Manufact 1999;30:871–7.
[24] Yan A-M, Marechal E, Nguyen-Dang H. A finite element model of mixed-mode delamination in laminated composites with an R-curve effect. Compos Sci Technol 2001;61:1413–27.
[25] Szekrényes A, Uj J. Beam and finite element analysis of quasi-unidirectional SLB and ELS specimens. Compos Sci Technol 2004;64:2393–406.
[26] Bao G, Ho S, Suo Z, Fan B. The role of material orthotropy in fracture specimens for composites. Int J Solids Struct 1992;29:1105–16.
[27] Williams JG. On the calculation of energy release rates for cracked laminates. Int J Fract 1988;36:101–19.
[28] Suo Z, Hutchinson JW. Interface crack between two elastic layers. Int J Fract 1990;43:1–18.
[29] Sundararaman V, Davidson BD. An unsymmetric end-notched flexure test for interfacial fracture toughness determination. Eng Fract Mech 1998;60:361–77.

[30] Sundararaman V, Davidson BD. An unsymmetric double cantilever beam test for interfacial fracture toughness determination. Int J Solids Struct 1997;34:799–817.
[31] Bruno D, Greco F. Mixed mode delamination in plates: a refined approach. Int J Solids Struct 2001;38:9149–77.
[32] Bruno D, Greco F. Delamination in composite plates: influence of shear deformability on interfacial debonding. Cement Concrete Compos 2001;23:33–45.
[33] Wang J, Qiao P. Interface crack between two shear deformable elastic layers. J Mech Phys Solids 2004;52:891–905.
[34] Raju IS, Crews Jr JH, Aminpour MA. Convergence of strain energy release rate components for edge-delaminated composite laminates. Eng Fract Mech 1988;30:383–96.
[35] Ducept F, Gamby D, Davies P. A mixed-mode failure criterion derived from tests of symmetric and asymmetric specimens. Compos Sci Technol 1999;59:609–19.
[36] Szekrényes A, Uj J. Application of the Winkler–Pasternak foundation in composite fracture mechanics—analysis of the DCB and SCB specimens. Int J Mech Sci, submitted for publication.
[37] Thamm F. Strength of plastic materials II, 1985 (in Hungarian).